

Energy-based Calibrated VAE with Test Time Free Lunch

Yihong Luo^{1,2}, Siya Qiu^{1,2}, Xingjian Tao^{1,3}, Yujun Cai⁴, Jing Tang^{1,2*}

¹ The Hong Kong University of Science and Technology (Guangzhou)

² The Hong Kong University of Science and Technology

³ South China University of Technology

⁴ Meta

Abstract

In this paper, we propose a novel Energy-Calibrated Generative Model that utilizes a Conditional EBM for enhancing Variational Autoencoders (VAEs). VAEs are sampling efficient but often suffer from blurry generation results due to the lack of training in the generative direction. On the other hand, Energy-Based Models (EBMs) can generate high-quality samples but require expensive Markov Chain Monte Carlo (MCMC) sampling. To address these issues, we introduce a Conditional EBM for calibrating the generative direction during training, without requiring it for test time sampling. Our approach enables the generative model to be trained upon data and calibrated samples with adaptive weight, thereby enhancing efficiency and effectiveness without necessitating MCMC sampling in the inference phase. We also show that the proposed approach can be extended to calibrate normalizing flows and variational posterior. Moreover, we propose to apply the proposed method to zero-shot image restoration via neural transport prior and range-null theory. We demonstrate the effectiveness of the proposed method through extensive experiments in various applications, including image generation and zero-shot image restoration. Our method shows state-of-the-art performance over single-step non-adversarial generation.

1. Introduction

Deep generative models, including generative adversarial nets (GANs) [9], variational autoencoders (VAEs) [23], flow-based generative models [4, 5], energy-based models (EBMs) [6, 44], and diffusion models [17], achieve excellent performance in a variety of applications.

Recently, likelihood-based models, such as VAEs, and EBMs, have gained more attention. Training of these models is accomplished by maximizing the data likelihood. Unlike GANs, likelihood-based models typically exhibit

greater stability during training and more faithfully cover modes in the data.

In particular, VAEs map the input data into a latent distribution and optimize the evidence lower bound (ELBO) on the data likelihood. The VAEs usually is computationally efficient, benefiting from efficient variational learning. VAEs also can generate samples in a single step with high efficiency. Moreover, VAEs do not suffer from architecture restrictions with expressivity limitations as normalizing flows face. However, VAEs do not optimize the generative side. Specifically, VAEs assume that the prior distribution in latent space (e.g., Gaussian distribution) matches the empirical distribution in latent space mapped from input data. Unfortunately, there is a gap between the two distributions in practice. As a result, these models struggle to generate sharp images, producing blurry or corrupted samples. To tackle this issue, in addition to designing more flexible prior distribution [1, 39, 48], some work [15, 34, 40] involves GANs, yielding unstable adversarial games, while NVAE [41] proposes to adjust BatchNorm [16] statistics based on prior distribution that improves the generation slightly.

On the other hand, EBMs model the unnormalized data density by assigning low energy to high-probability regions. The appeal of EBMs lies in their minimal restrictions on network architectures, unlike normalizing flows, thereby offering considerable potential for expressivity. EBMs also do not necessitate distribution assumptions in modeling, while VAEs usually assume the prior as Gaussian. In fact, EBMs have shown comparable state-of-the-art performance generative results among non-adversarial methods. However, a significant drawback of EBMs is the necessity for MCMC in training and sampling, which is computationally expensive, particularly when the energy is parameterized by neural networks.

In this paper, we propose a novel generative model termed Energy-based Calibrated VAE by involving a Conditional EBM to calibrate the VAE for better generation while keeping high sampling efficiency. The VAE is trained by

*Corresponding author.

ELBO and energy-based calibration. Specifically, to address the training of the generative side that is missing in VAE, we propose to incorporate the generated samples into training. That is, for generated data $\hat{\mathbf{x}}$ by the generative model, we use a conditional EBM to sample data $\tilde{\mathbf{x}}$ initialed with $\hat{\mathbf{x}}$ that approximates the input real data. Then, integrating the minimization of the distance between $\hat{\mathbf{x}}$ and $\tilde{\mathbf{x}}$ into training can calibrate the decoder. We show that the proposed model can be jointly trained by adopting the primal-dual method in a constrained formulation. Note that the EBM is involved in training (i.e., decoder calibration) only, and is not required during test time sampling.

Moreover, we show that the idea of energy-based calibration can be extended to calibrate the variational inference. We can sample \mathbf{z} from variational posterior, and then calibrate the \mathbf{z} by running MCMC on constructed conditional posterior $p(\tilde{\mathbf{z}}|\mathbf{z}, \mathbf{x})$ to obtain calibrated $\tilde{\mathbf{z}}$. Similarly, the encoder can be calibrated by minimizing the distance between \mathbf{z} and $\tilde{\mathbf{z}}$. In addition, we show that the energy-based calibration can also be extended to calibrate normalizing flows with large improvement.

Experimental results show that the proposed Calibrated VAE outperforms previous EBMs and state-of-the-art VAEs on image generation benchmarks in both low-resolution and high-resolution datasets by a large margin. Specifically, Calibrated VAE achieves state-of-the-art performance on CIFAR-10 among single-step non-adversarial models, outperforming single-step Consistency Models [38]. We also propose and show how to apply Calibrated VAE to image restoration in a zero-shot way by constructing neural transport prior and leveraging range-null space theory with competitive performance.

Our main contributions are summarized as follows.

1. We propose a new generative model termed Energy-based Calibrated VAE utilizing a conditional EBM to calibrate the VAE decoder to generate sharper samples without incurring extra costs during inference (i.e., test time MCMC-free sampling).
2. We show that the proposed energy-based calibration can be extended to enhance variational learning and normalizing flows.
3. We propose a zero-shot method for applying the proposed Energy-based Calibrated VAE in image restoration tasks by neural transport prior and range-null space theory.
4. We demonstrate the strong empirical results of the proposed Energy Calibrated Generative Model on various tasks, including image generation and image restoration.

2. Additional Related Work

Energy-based Models and Cooperative Learning. Our method shares some similarities with works that combine generative autoencoders and EBMs in different ways.

VAEBM [43] learns EBM upon a pre-trained NVAE [41], and [10] jointly learns EBM and VAE by an adversarial game instead of by MCMC, while our work is jointly trained without adversarial components. In addition, our learning algorithm bears some similarities to cooperative learning [45–47], which also employs EBM to teach the generator, but only in small images. However, the generator network in these approaches is purely trained upon *generated samples*, which can be quite biased. In contrast, our generative model (i.e., VAE) is trained upon data and generated samples, with adaptive weights. Furthermore, our work differs significantly from previous works in the way that our approach can discard MCMC during inference without adversarial components.

3. The Design of Energy Calibrated Generative Model

In this section, we first introduce some useful notations and preliminaries for building our model.

3.1. Notations

The notations used in this paper are defined as follows. Denote by \mathbf{x} the data and by \mathbf{z} the latent variable. Let \mathcal{X} be the data space and \mathcal{Z} be the latent space. Let $p_d(\mathbf{x})$ be the data distribution. Denote by $f_\alpha: \mathcal{X} \rightarrow \mathcal{Z}$ the encoder parameterized by α , and by $g_\beta: \mathcal{Z} \rightarrow \mathcal{X}$ the decoder parameterized by β . Let $p_\phi(\mathbf{x})$ be the probability function estimated by the generative model parameterized by ϕ over data space. Denote by $E_\omega: \mathcal{X} \rightarrow \mathbb{R}$ the energy function parameterized by ω . Distance function $d(\cdot, \cdot)$ is a metric defined over $\mathcal{X} \times \mathcal{X}$.

3.2. Preliminaries

Variational Auto-encoders VAE[22] adopts the encoder-decoder architecture with a prior distribution. To be more precise, VAE uses the encoder to parameterize the approximated posterior $q_\alpha(\mathbf{z}|\mathbf{x})$ and uses the decoder to parameterize the generator $p_\beta(\mathbf{x}|\mathbf{z})$ and the pre-defined or learnable prior distribution $p(\mathbf{z})$. α and β denote the parameters of neural networks. Those parameters are trained by maximizing the evidence lower bound (ELBO):

$$\log p_{\alpha, \beta}(\mathbf{x}) \geq \mathbb{E}_{q_\alpha(\mathbf{z}|\mathbf{x})}(\log p_\beta(\mathbf{x}|\mathbf{z})) - \text{KL}(q_\alpha||p(\mathbf{z})) \quad (1)$$

The first term is the reconstruction loss and the second term is the KL divergence between the approximated posterior distribution and the prior distribution.

Limitation in VAEs VAEs focus on maximizing the lower bound of data likelihood. However, the generative side is missing in the training objective, making it suffer from poor sampling quality. Specifically, the prior distribution usually can't match the real distribution of the latent space, assigned high density to low-density data, which is also called **prior hole issue**.

Energy-Based Models A deep EBM assumes that $p_\omega(\mathbf{x})$ is a gibbs distribution with the form $p_\omega(\mathbf{x}) = \exp(-E_\omega(\mathbf{x}))/L_\omega$, where L_ω is the corresponding normalizing constant. EBM is trained by minimizing the negative log-likelihood (NLL) $\mathcal{L}(\omega)$ such that

$$\mathcal{L}(\omega) = -\mathbb{E}_{p_d(\mathbf{x})}[\log p_\omega(\mathbf{x})] = -\mathbb{E}_{p_d(\mathbf{x})} \frac{\exp(-E_\omega(\mathbf{x}))}{L_\omega}. \quad (2)$$

In practice, we use mini-batch gradient descent to minimize $\mathcal{L}(\omega)$, i.e.,

$$\nabla \mathcal{L}(\omega) \approx \sum_{i=1}^n \frac{1}{n} \nabla E_\omega(\mathbf{x}_i^+) - \sum_{i=1}^n \frac{1}{n} \nabla E_\omega(\mathbf{x}_i^-), \quad (3)$$

where $\{\mathbf{x}_i^+\}_{i=1}^n$ is drawn from data distribution, and $\{\mathbf{x}_i^-\}_{i=1}^n$ is drawn from the model $p_\omega(\mathbf{x})$ by running MCMC sampling with K steps of Langevin dynamics, with given initial samples $\{\mathbf{x}_{i,0}^-\}_{i=1}^n$ and step size s :

$$\mathbf{x}_{k+1} = \mathbf{x}_k - \frac{s}{2} \nabla_{\mathbf{x}_k} E_\omega(\mathbf{x}_k) + \sqrt{s} \xi, \quad \text{where } \xi \sim \mathcal{N}(0, \mathbf{I}). \quad (4)$$

3.3. General Form of Energy-based Calibration

An issue with VAE is that the generative direction hasn't been trained during the training process, potentially leading to lower-quality output for the generated samples. To address this, we propose to incorporate the generated samples into the training. As the real data corresponding to the generated samples are unavailable, we suggest utilizing a short-run MCMC, initialized with the generated samples, to approximate the corresponding real data.

As the aim is to calibrate the samples, we suggest constructing a **Conditional EBM** to model the conditional density, i.e.,

$$p_\omega(\tilde{\mathbf{x}}|\mathbf{x}) = \frac{1}{L_\omega(\mathbf{x})} \exp(-E_\omega(\tilde{\mathbf{x}}) - d(\tilde{\mathbf{x}}, \mathbf{x})), \quad (5)$$

where $L_\omega(\mathbf{x}) = \int \exp(-E_\omega(\tilde{\mathbf{x}}) - d(\tilde{\mathbf{x}}, \mathbf{x})) d\tilde{\mathbf{x}}$ is the corresponding normalizing constant, \mathbf{x} is the generated samples from $p_\phi(\mathbf{x})$, E_ω is an unconditional EBM. Compared to direct model $p_\omega(\mathbf{x})$, the extra distance term in $p_\omega(\tilde{\mathbf{x}}|\mathbf{x})$ constrains the high-density area localized around generated samples \mathbf{x} , making it easier to be learned by the base generative model (i.e., VAE). Sampling from $p_\omega(\tilde{\mathbf{x}}|\mathbf{x})$ can be achieved by MCMC, i.e.,

$$\mathbf{x}_{k+1} = \mathbf{x}_k - \frac{s}{2} \left(\underbrace{\nabla_{\mathbf{x}_k} E_\omega(\mathbf{x}_k)}_{\text{direct to real}} + \underbrace{\nabla_{\mathbf{x}_k} d(\mathbf{x}_k, \mathbf{x})}_{\text{direct to origin}} \right) + \sqrt{s} \xi, \quad (6)$$

where $\xi \sim \mathcal{N}(0, \mathbf{I})$. For simplicity, we denote $\mathbf{x}^K = \text{MCMC}_\omega^K(\tilde{\mathbf{x}}|\mathbf{x})$. As the conditional EBM has not introduced new parameters, its learning can be achieved by learning the EBM E_ω as follows:

$$\begin{aligned} \nabla \mathcal{L}(\omega) &= \nabla \mathbb{E}_{p_d(\mathbf{x})} E_\omega(\mathbf{x}) - \nabla \mathbb{E}_{p_\omega(\mathbf{x})} E_\omega(\mathbf{x}) \\ &= \nabla \mathbb{E}_{p_d(\mathbf{x})} E_\omega(\mathbf{x}) - \nabla \mathbb{E}_{p_\phi(\mathbf{x})} \mathbb{E}_{p_\omega(\tilde{\mathbf{x}}|\mathbf{x})} E_\omega(\tilde{\mathbf{x}}). \end{aligned} \quad (7)$$

We show that the negative samples for learning EBMs can be drawn from the base generative model firstly, followed by running MCMC via conditional EBM by Eq. (6).

Then, we regard the $\tilde{\mathbf{x}}$ as calibrated samples, thus the generative side can be calibrated by minimizing the distance between \mathbf{x} and $\tilde{\mathbf{x}}$,

$$\begin{aligned} \mathcal{L}_{\text{calibration}} &= -\mathbb{E}_{p_\phi(\mathbf{x})} \mathbb{E}_{p_\omega(\tilde{\mathbf{x}}|\mathbf{x})} [\log p(\tilde{\mathbf{x}}|\mathbf{x})] \\ &= \mathbb{E}_{p_\phi(\mathbf{x})} \mathbb{E}_{p_\omega(\tilde{\mathbf{x}}|\mathbf{x})} d(\mathbf{x}, \tilde{\mathbf{x}}) \end{aligned} \quad (8)$$

We note that the calibration loss can also be considered as maximizing the likelihood of calibrated samples conditioned on generated samples. This MCMC can be regarded as a teacher, guiding the generative model to produce higher-quality generated samples. However MCMC introduces some random noise into training, making it impossible to perfectly match the calibrated samples, thus we suggest using a constrained optimization form as follows:

Definition 1 (Energy Calibrated Generative Model)

Given fixed margins ϵ_1 , the general optimization can be transformed into the following inequality-constrained optimization.

$$\min_{\phi, \omega} \mathcal{L}(\phi) + \mathcal{L}(\omega)$$

$$d(\tilde{\mathbf{x}}, \mathbf{x}) < \epsilon_1, \quad \forall \mathbf{x} \sim p_\phi(\mathbf{x}), \tilde{\mathbf{x}} = \text{MCMC}_\omega^K(\tilde{\mathbf{x}}|\mathbf{x}).$$

where $\mathcal{L}(\phi) = -\mathbb{E}_{p_d(\mathbf{x})} [\log p_\phi(\mathbf{x})]$ and $\mathcal{L}(\omega) = -\mathbb{E}_{p_d(\mathbf{x})} [\log p_\omega(\mathbf{x})]$.

We get a constrained optimization problem in Definition 1, which is hard to optimize directly, but we can consider it as a corresponding saddle-point problem as follows:

$$\max_{\lambda} \min_{\phi, \omega} \{ \mathcal{L}(\phi) + \mathcal{L}(\omega) + \lambda \mathcal{L}_{\text{con}}(\phi) \}, \quad (9)$$

where the constraint-related loss $\mathcal{L}_{\text{con}}(\theta)$ is defined as:

$$\mathcal{L}_{\text{con}}(\phi) = \mathbb{E}_{p_\phi(\mathbf{x})} \mathbb{E}_{p_\omega(\tilde{\mathbf{x}}|\mathbf{x})} [d(\mathbf{x}, \text{MCMC}_\omega^K(\tilde{\mathbf{x}}|\mathbf{x}) - \epsilon_1]. \quad (10)$$

The final challenge is the lack of access to the ground truth of data distribution. To tackle this issue, we consider the corresponding empirical optimization problem as follows:

$$\begin{aligned} &\max_{\lambda} \min_{\phi, \omega} \{ \hat{\mathcal{L}}(\phi) + \hat{\mathcal{L}}(\omega) + \lambda \mathcal{L}_{\text{con}}(\phi) \} \\ &= \max_{\lambda} \min_{\phi} \left\{ \sum_{i=1}^n -\log p_\phi(\mathbf{x}_i) + \sum_{i=1}^n -\log p_\omega(\mathbf{x}_i) \right. \\ &\quad \left. + \lambda \sum_{i=1}^n d(\hat{\mathbf{x}}, \text{MCMC}_\omega^K(\hat{\mathbf{x}}|\hat{\mathbf{x}})) \right\}, \end{aligned} \quad (11)$$

where \mathbf{x}_i is sampled from data, $\hat{\mathbf{x}}$ is sampled from the base generative model. MCMC is not necessary during test time sampling.

Concrete Algorithm To efficiently optimize the problem, we employ the primal-dual algorithm tailored for addressing the saddle-point problem corresponding to the constrained form. Specifically, in the *primal* step, the algorithm alternately optimizing parameters ω and ϕ by minimizing the empirical Lagrangian under a given dual variable λ , i.e.,

$$\begin{aligned}\omega_{t+1} &:= \arg \min_{\omega} \hat{\mathcal{L}}(\omega_t), \\ \phi_{t+1} &:= \arg \min_{\phi} \hat{\mathcal{L}}(\phi_t) + \lambda_t \hat{\mathcal{L}}_{\text{con}}(\phi_t).\end{aligned}\quad (12)$$

In practice, we perform stochastic gradient descent that derives concrete update step for θ and ϕ . On the other hand, in the *dual* step, we update λ as follows,

$$\lambda_{t+1} := \max \left\{ \lambda_t + \eta \cdot (\hat{\mathcal{L}}_{\text{con}} - \epsilon), 0 \right\}, \quad (13)$$

where η is the learning rate of dual step.

Algorithm 1 gives the pseudo-code of our primal-dual algorithm for optimizing the generative model parameters ϕ , and EBMs parameters ω . Compared with using stochastic gradient descent directly in the constrained optimization problem in Definition (1), the primal-dual algorithm can dynamically tune λ to avoid introducing extra hyperparameters (which may serve as an early-stopping condition, e.g., $\lambda = 0$), and can provide convergence guarantees with sufficiently long training using sufficiently small step size [2].

3.4. Energy-based Calibrated VAE

A latent generator model decomposes the joint distribution of (\mathbf{x}, \mathbf{z}) as $p_{\beta, \theta}(\mathbf{x}, \mathbf{z}) = p_{\beta}(\mathbf{x}|\mathbf{z})p_{\theta}(\mathbf{z})$.

The model can be trained by maximizing the log-likelihood $\mathcal{L} = \mathbb{E}_{p_d(\mathbf{x})} \log p_{\beta, \theta}(\mathbf{x})$. This maximization can be achieved by gradient ascent where the gradient can be obtained from:

$$\begin{aligned}\nabla \log p_{\beta, \theta}(\mathbf{x}) &= \frac{1}{p_{\beta, \theta}(\mathbf{x})} \nabla p_{\beta, \theta}(\mathbf{x}) \\ &= \int \nabla \log p_{\beta, \theta}(\mathbf{x}, \mathbf{z}) \frac{p_{\beta, \theta}(\mathbf{x}, \mathbf{z})}{p_{\beta, \theta}(\mathbf{x})} d\mathbf{z} \\ &= \mathbb{E}_{p_{\beta, \theta}(\mathbf{z}|\mathbf{x})} \nabla \log p_{\beta, \theta}(\mathbf{x}, \mathbf{z})\end{aligned}\quad (14)$$

The term $\nabla \log p_{\beta, \theta}(\mathbf{x}, \mathbf{z})$ can be easily computed based on the form of $\log p_{\beta, \theta}(\mathbf{x}, \mathbf{z})$. However, estimating the expectation needs sampling from intractable $p_{\beta, \theta}(\mathbf{z}|\mathbf{x})$.

Variational Learning Instead of sampling from intractable posterior $p_{\beta, \theta}(\mathbf{z}|\mathbf{x})$, VAEs propose using a variational inference $q_{\alpha}(\mathbf{z}|\mathbf{x})$ with parameters α to approximate the posterior. This makes the maximizing objective of VAEs no longer be an exact likelihood, but the lower-bound termed ELBO. Thus we need to replace the training objective $\mathcal{L}(\phi)$ in Energy-Calibrated Generative Models by the ELBO, where $\phi = \{\beta, \alpha, \theta\}$ is the total parameter set of each component in VAEs. Moreover, as the

$p_{\phi}(\mathbf{x}) = \int p_{\beta}(\mathbf{x}|\mathbf{z})p_{\theta}(\mathbf{z})d\mathbf{z}$ of VAEs is intractable. Thus we should sample \mathbf{z} from prior $p_{\theta}(\mathbf{z})$ and then decode it to obtain generated samples $\mathbf{x} = g_{\beta}(\mathbf{z})$. Specifically, given the generated samples and the calibrated samples, the learning of $\phi = \{\beta, \alpha, \theta\}$ should be divided into three parts related to the Decoder β , Encoder α , and Prior θ as follows:

$$\begin{aligned}\beta &= \arg \min_{\beta} \{ \lambda \mathcal{L}_{\text{con}}(\beta) - \log \mathbb{E}_{q_{\alpha}(\mathbf{z}|\mathbf{x})} p_{\beta}(\mathbf{x}|\mathbf{z}) \} \\ \alpha &= \arg \min_{\alpha} \{ KL(q_{\alpha}(\mathbf{z}|\mathbf{x}) || p_{\theta}(\mathbf{z})) - \log \mathbb{E}_{q_{\alpha}(\mathbf{z}|\mathbf{x})} p_{\beta}(\mathbf{x}|\mathbf{z}) \} \\ \theta &= \arg \min_{\theta} \log \mathbb{E}_{\mathbf{x}} \mathbb{E}_{q_{\alpha}(\mathbf{z}|\mathbf{x})} p_{\theta}(\mathbf{z})\end{aligned}\quad (15)$$

where the update of EBMs component ω and λ keep the same.

Limitation: Although variational learning can be efficiently trained, it leads to a lower bound learning of data likelihood. The gap is the KL divergence between variational posterior $q_{\alpha}(\mathbf{z}|\mathbf{x})$ and posterior $p_{\beta, \theta}(\mathbf{z}|\mathbf{x})$ which is not explicitly minimized in variational training, just like the training of the generative side is missing in vanilla VAEs.

Energy-based Calibrated Variational Learning Similar to calibrating the generative side as proposed in Sec. 3.3, we propose to incorporate the calibration of the variational posterior $q_{\alpha}(\mathbf{z}|\mathbf{x})$ into training. We first construct the conditional density $p_{\beta, \theta}(\tilde{\mathbf{z}}|\mathbf{z}, \mathbf{x})$ as follows:

$$p_{\beta, \theta}(\tilde{\mathbf{z}}|\mathbf{z}, \mathbf{x}) = p_{\beta, \theta}(\tilde{\mathbf{z}}|\mathbf{x}) \times \exp(-d(\tilde{\mathbf{z}}, \mathbf{z}))/L_{\beta, \theta}(\mathbf{z}) \quad (16)$$

where $p_{\beta, \theta}(\tilde{\mathbf{z}}|\mathbf{x})$ is the posterior, $L_{\beta, \theta}(\mathbf{z})$ is corresponding normalizing constant. The conditional density is constructed by adding the distance term to constrain the calibrated \mathbf{z} to be close to \mathbf{z} . And the sampling can be by MCMC with Langevin dynamics. Given a step size $s > 0$ and an initial value \mathbf{z}_0 , the Langevin dynamics iterates:

$$\mathbf{z}_{k+1} = \mathbf{z}_k - \frac{s}{2} \nabla_{\mathbf{z}_k} \log p_{\beta, \theta}(\mathbf{z}_k|\mathbf{z}_0, \mathbf{x}) + \sqrt{s} \xi,$$

where $\xi \sim \mathcal{N}(0, \mathbf{I})$ and the \mathbf{z}_0 is proposed to be sampled from variational posterior $q_{\alpha}(\mathbf{z}|\mathbf{x})$, thus the \mathbf{z}_K can be considered as calibrated \mathbf{z} . Note the $\nabla \log p_{\beta, \theta}(\mathbf{z}|\mathbf{x})$ can be easily obtained by following form: $\nabla_{\mathbf{z}} \log p_{\beta, \theta}(\mathbf{z}|\mathbf{x}) = \nabla_{\mathbf{z}} \log p(\mathbf{x}, \mathbf{z}) + \nabla_{\mathbf{z}} \log p(\mathbf{x}) = \nabla_{\mathbf{z}} \log p(\mathbf{x}, \mathbf{z})$.

Once the MCMC Calibrated \mathbf{z}_K is obtained, we can conduct the constrained learning formulation similar to Sec. 3.3. We here directly give the corresponding saddle-point problem:

$$\begin{aligned}\mathcal{L}(\phi = \{\alpha, \beta, \theta\}) &= -\mathbb{E}_{p_d(\mathbf{x})} \mathbb{E}_{q_{\alpha}(\mathbf{z}|\mathbf{x})} \log p_{\beta, \theta}(\mathbf{x}, \mathbf{z}) \\ &\quad + \lambda_1 \times \mathcal{L}_{\text{con}}(\beta) + \lambda_2 \times \mathcal{L}_{\text{con}}(\alpha),\end{aligned}\quad (17)$$

where $\mathcal{L}_{\text{con}}(\alpha) = -\mathbb{E}_{q_{\alpha}(\mathbf{z}|\mathbf{x})} \mathbb{E}_{p_{\beta, \theta}(\tilde{\mathbf{z}}|\mathbf{z}, \mathbf{x})} \log p(\tilde{\mathbf{z}}|\mathbf{z}) = \mathbb{E}_{q_{\alpha}(\mathbf{z}|\mathbf{x})} d(\mathbf{z}, \text{MCMC}_{\beta, \theta}^K(\tilde{\mathbf{z}}|\mathbf{z}))$. Given the saddle-point for-

mulation, the learning and calibration of the encoder parameterized by α can be achieved as follows:

$$\alpha = \alpha - \nabla_{\alpha} [\text{KL}(q_{\alpha}(\mathbf{z}|\mathbf{x})||p_{\theta}(\mathbf{z})) - \log \mathbb{E}_{q_{\alpha}(\mathbf{z}|\mathbf{x})} p_{\beta}(\mathbf{x}|\mathbf{z}) - \lambda_2 \times \mathbb{E}_{q_{\alpha}(\mathbf{z}|\mathbf{x})} \mathbb{E}_{p_{\beta, \theta}(\mathbf{z}|\mathbf{z}, \mathbf{x})} \log p(\mathbf{z}|\mathbf{z})] \quad (18)$$

The update of the rest parameters $\{\beta, \theta, \omega\}$ remains the same, while the λ_i ($i=1,2$) is updated by Eq. (13).

3.5. Extend to Energy-based Calibrated Normalizing Flow

The Energy-Calibrated Normalizing Flow can be easily formed, as normalizing flow h_{ϕ} directly models the data likelihood $p_{\phi}(\mathbf{x}) = p_{\mathbf{z}}(\mathbf{z}) \times \left| \det \left(\frac{\partial h_{\phi}}{\partial \mathbf{z}} \right) \right|$, where h_{ϕ} is a invertible transformation. Thus we just need to use the negative log-likelihood $-\mathbb{E}_{p_d(\mathbf{x})} \log p_{\phi}(\mathbf{x})$ estimated by normalizing flow to serve as the $\mathcal{L}(\phi)$, while other components keep the same.

3.6. Applying to Zero-Shot Image Restoration

In this section, we present the application of our method in zero-shot image restoration tasks, inspired by recent works [42] that employ the diffusion model and the Range-Null space theory for similar purposes.

We start by briefly reviewing the necessary background. Given a known linear operator $\mathbf{A} \in \mathbb{R}^{D_1 \times D_2}$, there exists pseudo-inverse $\mathbf{A}^{\dagger} \in \mathbb{R}^{D_2 \times D_1}$ that satisfies $\mathbf{A}\mathbf{A}^{\dagger}\mathbf{A} = \mathbf{A}$. Considering degraded image: $\mathbf{y} = \mathbf{A}\mathbf{x}$. For any prediction $\hat{\mathbf{x}}_r$, we let $\hat{\mathbf{x}} = \mathbf{A}^{\dagger}\mathbf{y} + (\mathbf{I} - \mathbf{A}^{\dagger}\mathbf{A})\hat{\mathbf{x}}_r$, then immediately gives: $\mathbf{A}\hat{\mathbf{x}} = \mathbf{A}\mathbf{A}^{\dagger}\mathbf{y} + \mathbf{0} = \mathbf{A}\mathbf{x}$, which we make predicted images have the same degradation as original images. This can be regarded as \mathbf{x}_r predicting the zero-space while remaining the original rang-space $\mathbf{A}\mathbf{x}$. For getting the $\hat{\mathbf{x}}_r$, we can employ $\mathbf{A}^{\dagger}\mathbf{y}$ which is the range-space part of \mathbf{x} as biased ground truth and build a joint distribution

$$p_{\beta, \theta}(\mathbf{A}^{\dagger}\mathbf{y}, \mathbf{z}) = p_{\theta}(\mathbf{z})p(\mathbf{A}^{\dagger}\mathbf{y}|\mathbf{A}^{\dagger}\mathbf{A}g_{\beta}(\mathbf{z})). \quad (19)$$

However the $p_{\theta}(\mathbf{z})$ may not be powerful enough to handle image restoration. Recall that we have an EBM in data space, hence we can construct a more powerful prior via neural transport, i.e.,

$$\begin{aligned} p_{\theta, \omega}(\mathbf{z}) &\propto \exp(-E_{\omega}(g_{\beta}(\mathbf{z})))p_{\theta}(\mathbf{z}) \\ &\propto \exp(-E_{\beta, \omega}(\mathbf{z}))p_{\theta}(\mathbf{z}) \end{aligned} \quad (20)$$

This is achieved by transporting \mathbf{z} to data space via decoder, then the EBM defined in data space is used, finally, the EBM defined in latent space for enhancing prior is well-constructed. By substituting the prior in Eq. (20) into Eq. (19), the new joint likelihood is obtained. Then we run MCMC on \mathbf{z} to maximize the biased joint likelihood, i.e.,

$$g_{\beta}(\mathbf{z}_r^{k+1}) = g_{\beta}(\mathbf{z}_r^k) - \frac{s}{2} \nabla_{\mathbf{z}_r^k} \log p_{\theta, \beta, \omega}(\mathbf{A}^{\dagger}\mathbf{y}, \mathbf{z}_r^k) + \sqrt{s}\xi \quad (21)$$

Table 1. Generative performance on CIFAR-10 and STL-10. The \dagger means without extra hyper-parameters tuning. The $*$ means we evaluate the FID by officially released pre-trained checkpoint.

	Model	NFE \downarrow	FID \downarrow	Times (s) \downarrow
Score-based	NCSN [36]	1000	25.32	107.9
	Denoising Diffusion [14]	1000	3.17	80.5
	Consistency Models (LPIPS) [38]	1	8.70	-
GAN-based	SN-GAN [30]	1	21.7	-
	AutoGAN [8]	1	12.4	-
	StyleGAN2 w/o ADA [19]	1	9.9	0.04
VAEs+GANs	VAE+GAN [34]	1	39.8	-
	DC-VAE [34]	1	17.9	-
EBMs+GANs	FlowCE [7]	1	37.3	-
	Divergence Triangle [10]	1	30.1	-
Flow-based	Glow [21]	1	48.9	-
	SurVAE Flow [31]	1	49.03	-
NVAE-family	NVAE [41]	1	50.97	0.36
	NCP-VAE [1]	1	24.08	8.79
Energy-based	IGEBM [6]	60	40.58	-
	CoopFlow [47]	31	15.80 (26.54 † *)	-
	CoopFlow w/o MCMC	1	79.45*	-
	NT-EBM w/ Flow [32]	-	78.12	-
	CLEL-Large [24]	1200	8.61	-
	VAEBM [43]	16	12.19	8.79
Ours	Calibrated VAE	1	8.02	0.03
	Calibrated Flow	1	31.12	0.37
Ablations	Calibrated VAE w/ MCMC	31	8.31	0.52
	Calibrated Flow w/ MCMC	31	22.74	0.86
	VAE	1	105.71	0.03
	Flow	1	91.33	0.37

Where $\xi \sim \mathcal{N}(0, \mathbf{I})$, \mathbf{z}_r^0 can be initiated by sampling from $p_{\theta}(\mathbf{z})$. In practice, the linear degraded operator \mathbf{A} has various corresponding image restoration tasks, such as colorization, super-resolution, and inpainting. See Appendix B for concrete forms of \mathbf{A} and \mathbf{A}^{\dagger} . It's worth noting that our proposed method doesn't need extra training for those tasks.

4. Experiment

In this section, we conduct comprehensive experiments to evaluate the proposed Energy-based Calibrated VAE. We also evaluate the extension of Energy-based calibration to normalizing flow and variational inference. We use a simple ResNet [12] similar to used in VAEBM [43] or CLEL [24] as energy functions E_{ω} with 15 or 30 MCMC steps in all experiments. We adopt Fréchet Inception Distance (FID) score [13] as quantitative metrics in most experiments. Please note that by default, our proposed model does not incorporate the use of MCMC in test time, unless specifically indicated otherwise. The distance metric is chosen to be Mean Squared Error (MSE) as default.

4.1. Image Generation

In this section, we evaluate Energy-based Calibrated VAE on five datasets, including CIFAR-10 [49], STL-10 [3], CelebA [27], LSUN Church-64 [49], and CelebA-HQ-256 [28]. The backbone similar to that proposed in FastGAN [26] is used in experiments. See Appendix D for more experiment setting details. We show qualitative results in Fig. 1. See Appendix G for more qualitative results and qualitative comparison to other models. The quantita-



Figure 1. Random generated samples from Energy-based Calibrated VAE. For CelebA HQ 256 and CelebA, we picked out samples for diversity.



Figure 2. Qualitative results of Zero-Shot Image Restoration (Colorization, Inpainting, 4× Super-Resolution).

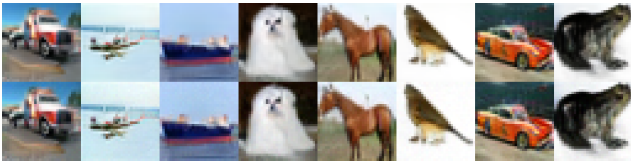


Figure 3. Comparison of **Calibrated VAE** (Top) and **Calibrated VAE (w/ MCMC)** (Bottom) on CIFAR-10. Best viewed when zoomed in.

tive results are reported in Tab. 1, Tab. 2, Tab. 3 and Tab. 8, with the best results for GANs or Score-models, as well as for other models respectively highlighted in bold.

Our results are comparable to advanced GANs and Score-based Models, outperforming NVAE-family (including NVAE, NCP-VAE and VAEBM) and GLOW, the most advanced Hierarchical VAE and flows, respectively, by a significant margin on all datasets, despite using much smaller latent space, and much fewer training resources.

Table 2. Generative performance on CelebA.

Model	FID↓
NCSNv2 [37]	26.86
COCO-GAN [25]	4.0
QA-GAN [33]	6.42
Divergence Triangle [10]	24.7
VAEBM [43]	5.31
NCP-VAE [1]	5.25
NVAE [41]	14.74
Calibrated VAE (Ours)	4.20

Table 3. Generative performance on CelebA-HQ.

Model	FID↓
ALAE [35]	19.21
DC-VAE [34]	15.81
PGGAN [18]	8.03
GLOW [21]	68.93
VAEBM [43]	20.38
NCP-VAE [1]	24.79
NVAE [41]	45.11
Calibrated VAE (Ours)	13.62

Table 4. Quantitative results Calibrated posterior on CIFAR-10.

Model	FID↓	MSE↓	ELBO↑
VAE	105.71	0.0247	-961.15
+ Calibrated posterior	103.42	0.0206	-363.25
Calibrated VAE	8.02	0.0199	595.98
+ Calibrated posterior	8.57	0.0175	1021.80

Our results also outperform existing EBMs, with a single-step generation manner. Additionally, Our results outperform the Consistency Models with Learned Perceptual Image Patch Similarity (LPIPS) which is the SOTA on single-step non-adversarial generation. Note that LPIPS is considered to hack FID to some extent, which is not used in our approach. And on Church 64, we obtain FID 7.52 which significantly beat NVAE’s 41.3 and VAEBM’s 13.51. Also, our results even outperform DC-VAE [34] across datasets, a powerful VAE with an adversarial part.

Compared to other EBMs: The proposed method presents a crucial, clear difference from existing methods: we demonstrate that it is possible to drop MCMC steps during test time sampling without compromising the quality of generation. And the FID is even better without MCMC. This is likely because MCMC introduces noise at each step which cannot be perfectly denoised (See Fig. 3), resulting in noise still present in the image. In contrast, the decoder minimizes the distance $\mathbb{E}_{\mathbf{x}} d(\tilde{\mathbf{x}}, \mathbf{x})$, assuming $\tilde{\mathbf{x}} = \mathbf{y} + \xi$, where ξ is random noise without any information. The minimum is ideally achieved at $\mathbf{x} = \mathbf{y}$, allowing the decoder to act as a filter and output sharp images without noise. Moreover, as observed, most previous EBMs [6, 43, 47] need to tune MCMC steps and step size carefully during inference to achieve high performance (e.g., CoopFlow[†] in Tab. 1), while our method does not need extra hyper-parameters tuning as even no MCMC required during inference.

The Effect of Energy-based Calibrated Variational Learning We evaluate Energy-based Calibrated Variational Learning on CIFAR-10. As shown in Tab. 4, the calibrated posterior consistently improves the ELBO and MSE of related baseline VAE and Calibrated VAE. This indicates that the calibrated posterior can provide a more accurate posterior for better likelihood maximization. However, the Calibrated VAE with Calibrated posterior shows a little bit of FID degradation, indicating that the likelihood is not always consistent with generation quality. Interestingly, we found the calibrated VAE also improves the ELBO and MSE compared to VAE, although we only calibrate the generative side. This may be highly due to the energy-based calibration effectively improving the ability to map latent space to data space and reducing the gap between prior and aggregated posterior.

The Effect of Energy-based Calibrated Normalizing Flow We also evaluate the Energy-based Calibrated Normalizing Flow on CIFAR-10. As shown in Tab. 1. We use Glow as the flow architecture. The Calibrated Flow outperforms existing flows in single-step generation. Note that we also outperform the FlowCE which is trained by playing an adversarial game. However, we found that in the case of calibrated flow, the MCMC still performs an important role in improving generative performance. Specifically, calibrated flow w/ MCMC significantly improves the FID from 31.12 to 22.74. We believe that this is due to the expressivity limitations of invertible transformations in flows. However, compared to CoopFlow which also combines flows and EBMs, our calibrated flow beat CoopFlow without MCMC by a large margin, demonstrating the effectiveness of the proposed calibrated flow. Note that the 15.8 FID achieved by CoopFlow needs extra hyper-parameter tuning, its result (26.54 FID) without extra tuning is worse than ours w/ MCMC (22.74 FID).

Table 5. Sampling efficiency and training cost on CIFAR-10. Time is the seconds took to generate 50 images.

Model	FID↓	Latent dim↓	Time↓	GPU days ↓	GPU-Type
NCSN	25.32	3072	107.9	-	-
GLOW [31]	48.9	3072	-	60	-
SurVAE Flow [31]	49.03	1536	-	7	TITAN-X
NVAE [41]	50.97	153600	0.36	18.3	32G-V100
NCP-VAE [1]	24.08	153600	-	34.5	32G-V100
VAEBM [43]	12.19	153600	8.79	≥18.3	32G-V100
Calibrated VAE (ours)	8.02	128	0.03	3	RTX-3090
Calibrated VAE w/ MCMC (ours)	8.31	128	0.52	3	RTX-3090

Table 6. Quantitative results of image restoration on CelebA-HQ.

Model	4× SR	Colorization
	PSNR↑ / FID↓	Cons↓ / FID↓
PULSE [29]	22.7 / 40.3	N/A
DDRM [20]	31.6 / 31.0	456 / 31.2
DDNM [42]	31.6 / 22.3	26.2 / 26.4
Calibrated VAE (ours)	28.8 / 30.4	0.004 / 13.3

4.2. Sampling Efficiency And Training Cost

Although the score-based model and NVAE’s variants have shown outstanding sample quality, their sampling speed is limited by the necessity of expensive MCMC sampling steps. As shown in Tab. 5, the generation by Calibrated VAE, in contrast, takes just one pass, making it hundreds of and thousands of times faster than NCSN and VAEBM, respectively. Notably, even after performing MCMC steps, our method still only requires 0.52 seconds to generate 50 samples. This is because our energy network is lightweight and only requires 30 MCMC steps on the data space, while VAEBM runs MCMC in (\mathbf{x}, \mathbf{z}) space which requires backward through its heavy decoder at each step. Furthermore, due to the extremely large scale of latent variables used in NVAE-family and previous flows, yielding challenges in learning, they need at least 7 GPU days to be trained on CIFAR-10, while our model only needs around 3 GPU days.

4.3. Image Restoration

Here we show that well-trained Energy Calibrated Generative Model is able to be zero-shot used in image restoration as described in Sec. 3.6. The Qualitative results are shown in Fig. 2. Our model can successfully restore those images with high quality and consistency. Following the setting as in [42], we compare our method with strong zero-shot baselines, using metrics FID, PSNR, and Consistency[42] (i.e., $\|\mathbf{A}\hat{\mathbf{x}} - \mathbf{A}\mathbf{x}\|_1$). As shown in Tab. 6, we outperform GAN-based PULSE [29] and compete with diffusion-based DDNM [42] and DDRM [20], which confirms our model provides competitive performance.

4.4. Ablation Study

All experiments here are performed on CIFAR-10 for faster training. Experimental settings can be found in Appendix F.

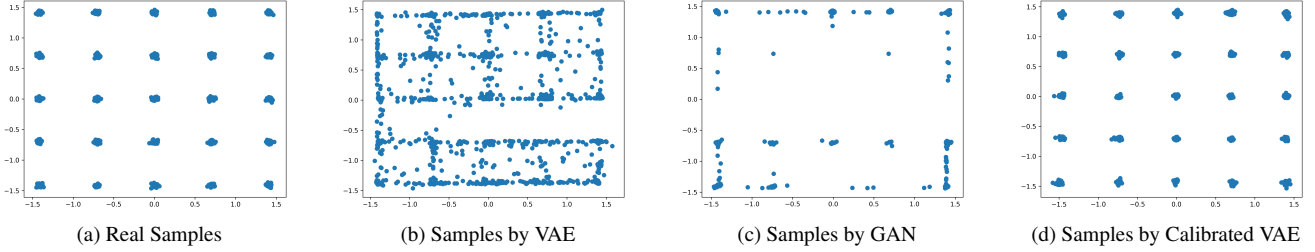


Figure 4. Qualitative results on the 25-Gaussians dataset.

Table 7. Comparison for FID on CIFAR-10 between several related training methods.

Model	FID↓
Calibrated VAE	8.02
Calibrated VAE w/o primal-dual	8.63
VAE	105.71
EBM	45.52
EBM init w/ VAE samples	44.90
VAE + GAN	38.61

The Effect of Calibration The proposed method is calibrating generative models by incorporating generated samples into training. Hence, a natural question is what is the performance of single generative model and train generative model and EBMs as two independent components? We compare the proposed Calibrated VAE with other three related baselines i.e., VAE, EBM, and EBM initialized with pre-trained VAE samples. As shown in Table. 7, we significantly outperform these three variants by a huge margin. Note that there is almost none benefit of initializing EBM with pre-trained VAE samples, implying the effectiveness of calibration.

Energy-based Calibration v.s. Adversarial-based Calibration The gradient for updating EBMs E_ω is similar to the gradient updates of WGAN’s discriminator. However, a critical distinction lies in the sampling methodology. EBMs utilize MCMC to draw samples from E_ω , whereas WGAN uses a generator to produce negative samples. The update mechanism also differs. WGAN plays an adversarial game to update both the generator and discriminator, while we update EBMs by maximizing the likelihood and we update the generative model by maximizing adaptive weight between data likelihood (or the lower bound) and conditional likelihood on calibrated samples ($\log p(\tilde{\mathbf{x}}|\mathbf{x})$). Thus, a related variant of Calibrated VAE is updating the decoder g_β by both ELBO and WGAN training objectives. We compare the adversarial variant with the proposed Calibrated VAE. As shown in Table. 7, the adversarial variant achieves similar results (**38.61 FID**) to the VAEs+GANs (**39.8 FID**) in DC-VAE which is significantly worse than the proposed Calibrated VAE (**8.02 FID**), highlighting the advantage of our method compared to adversarial training.

The Effect of Primal-Dual. We firstly emphasize that primal-dual has advantages with theoretical guarantees in constrained learning [2]. This section is for empirically showing the impact intuitively. As shown in Tab. 7, in comparison to primal-dual, the naive stochastic gradient descent (without dual variable λ) algorithm yields worse results.

4.5. Extra Studies

Mode Coverage: We evaluate the mode coverage of our model on the popular 25-Gaussians. This 2D toy dataset is also used in previous work [43]. We train our Calibrated VAE with 15 MCMC steps and compare it to other models in Figure. 4. The VAE’s encoder, decoder, and energy function both consist of four linear layers with 256 hidden units. The latent dimension is 20. We observe that the vanilla VAEs can not produce good samples, lots of samples are significantly out of modes. In contrast, our Calibrated VAE successfully calibrated the sampling distribution with all modes covered and high-quality samples. We also train a GAN with similar networks for comparison. We observe that GAN suffers severely from mode collapse. Moreover, as the true distribution is available, we also evaluate the likelihood of 100000 generated samples by models with true data density. Our Calibrated VAE obtains **-1.07 nats** which significantly improves the likelihood obtained by VAE which is **-1.78 nats**. For reference, the likelihood of 100000 real data under real density is **-1.04 nats**

5. Conclusion

The proposed Energy-based Calibrated VAE shows promising results over multiple datasets with high computational efficiency, significantly reducing the gap with GANs. We show that MCMC can be dropped after the generative model is calibrated while keeping high performance. We also show the proposed energy-based calibration can enhance normalizing flows and variational posterior. Additionally, we propose and show that Calibrated VAE can effectively solve image restoration in a zero-shot manner. In terms of efficiency, Calibrated VAE can be trained by single GPU and is fast to converge, addressing the intensive computational resources consumption problem of previous state-of-the-art VAEs.

References

- [1] Jyoti Aneja, Alex Schwing, Jan Kautz, and Arash Vahdat. A contrastive learning approach for training variational autoencoder priors. *Advances in Neural Information Processing Systems*, 34, 2021. 1, 5, 6, 7
- [2] Luiz FO Chamon, Santiago Paternain, Miguel Calvo-Fullana, and Alejandro Ribeiro. Constrained learning with non-convex losses. *arXiv:2103.05134*, 2021. 4, 8
- [3] Adam Coates, Andrew Ng, and Honglak Lee. An analysis of single-layer networks in unsupervised feature learning. In *AISTATS*, pages 215–223, 2011. 5
- [4] Laurent Dinh, David Krueger, and Yoshua Bengio. NICE: non-linear independent components estimation. In *3rd International Conference on Learning Representations, ICLR 2015, San Diego, CA, USA, May 7-9, 2015, Workshop Track Proceedings*, 2015. 1
- [5] Laurent Dinh, Jascha Sohl-Dickstein, and Samy Bengio. Density estimation using real nvp. *arXiv preprint arXiv:1605.08803*, 2016. 1
- [6] Yilun Du and Igor Mordatch. Implicit generation and modeling with energy based models. In *Advances in Neural Information Processing Systems*, pages 3608–3618, 2019. 1, 5, 7
- [7] Ruiqi Gao, Erik Nijkamp, Diederik P Kingma, Zhen Xu, Andrew M Dai, and Ying Nian Wu. Flow contrastive estimation of energy-based models. In *Proceedings of the IEEE/CVF Conference on Computer Vision and Pattern Recognition*, pages 7518–7528, 2020. 5
- [8] Xinyu Gong, Shiyu Chang, Yifan Jiang, and Zhangyang Wang. Autogan: Neural architecture search for generative adversarial networks. In *ICCV*, 2019. 5, 11
- [9] Ian Goodfellow, Jean Pouget-Abadie, Mehdi Mirza, Bing Xu, David Warde-Farley, Sherjil Ozair, Aaron Courville, and Yoshua Bengio. Generative adversarial nets. *Advances in neural information processing systems*, 27, 2014. 1
- [10] Tian Han, Erik Nijkamp, Linqi Zhou, Bo Pang, Song-Chun Zhu, and Ying Nian Wu. Joint training of variational autoencoder and latent energy-based model. In *Proceedings of the IEEE/CVF Conference on Computer Vision and Pattern Recognition*, pages 7978–7987, 2020. 2, 5, 6
- [11] Hao He, Hao Wang, Guang-He Lee, and Yonglong Tian. Probgan: Towards probabilistic gan with theoretical guarantees. In *ICLR*, 2019. 11
- [12] Kaiming He, Xiangyu Zhang, Shaoqing Ren, and Jian Sun. Deep residual learning for image recognition. In *Proceedings of the IEEE Conference on Computer Vision and Pattern Recognition (CVPR)*, 2016. 5
- [13] Martin Heusel, Hubert Ramsauer, Thomas Unterthiner, Bernhard Nessler, and Sepp Hochreiter. Gans trained by a two time-scale update rule converge to a local nash equilibrium. In *Advances in neural information processing systems*, pages 6626–6637, 2017. 5
- [14] Jonathan Ho, Ajay Jain, and Pieter Abbeel. Denoising diffusion probabilistic models. *arXiv preprint arXiv:2006.11239*, 2020. 5
- [15] Huaibo Huang, Ran He, Zhenan Sun, Tieniu Tan, et al. Introvae: Introspective variational autoencoders for photographic image synthesis. *Advances in neural information processing systems*, 31, 2018. 1
- [16] Sergey Ioffe and Christian Szegedy. Batch normalization: Accelerating deep network training by reducing internal covariate shift. *CoRR*, abs/1502.03167, 2015. 1
- [17] Ho Jonathan, Ajay Jain, and Pieter Abbeel. Denoising diffusion probabilistic models. *Advances in Neural Information Processing Systems*, 33:6840–6851, 2020. 1
- [18] Tero Karras, Timo Aila, Samuli Laine, and Jaakko Lehtinen. Progressive growing of GANs for improved quality, stability, and variation. In *International Conference on Learning Representations*, 2018. 6
- [19] Tero Karras, Miika Aittala, Janne Hellsten, Samuli Laine, Jaakko Lehtinen, and Timo Aila. Training generative adversarial networks with limited data. *arXiv preprint arXiv:2006.06676*, 2020. 5
- [20] Bahjat Kavar, Michael Elad, Stefano Ermon, and Jiaming Song. Denoising diffusion restoration models. In *Advances in Neural Information Processing Systems*, 2022. 7
- [21] Diederik P Kingma and Prafulla Dhariwal. Glow: Generative flow with invertible 1x1 convolutions. *arXiv preprint arXiv:1807.03039*, 2018. 5, 6
- [22] Diederik P Kingma and Max Welling. Stochastic gradient vb and the variational auto-encoder. In *Second International Conference on Learning Representations, ICLR*, page 121, 2014. 2
- [23] Diederik P Kingma and Max Welling. Auto-encoding variational bayes. In *The International Conference on Learning Representations (ICLR)*, 2014. 1
- [24] Hankook Lee, Jongheon Jeong, Sejun Park, and Jinwoo Shin. Guiding energy-based models via contrastive latent variables. In *The Eleventh International Conference on Learning Representations*, 2023. 5
- [25] Chieh Hubert Lin, Chia-Che Chang, Yu-Sheng Chen, Da-Cheng Juan, Wei Wei, and Hwann-Tzong Chen. Coco-gan: generation by parts via conditional coordinating. In *Proceedings of the IEEE International Conference on Computer Vision*, pages 4512–4521, 2019. 6
- [26] Bingchen Liu, Yizhe Zhu, Kunpeng Song, and Ahmed Elgammal. Towards faster and stabilized gan training for high-fidelity few-shot image synthesis. In *International Conference on Learning Representations*, 2020. 5
- [27] Ziwei Liu, Ping Luo, Xiaogang Wang, and Xiaoou Tang. Deep learning face attributes in the wild. In *ICCV*, 2015. 5
- [28] Ziwei Liu, Ping Luo, Xiaogang Wang, and Xiaoou Tang. Deep learning face attributes in the wild. In *Proceedings of the IEEE international conference on computer vision*, pages 3730–3738, 2015. 5
- [29] Sachit Menon, Alexandru Damian, Shijia Hu, Nikhil Ravi, and Cynthia Rudin. Pulse: Self-supervised photo upsampling via latent space exploration of generative models. In *Proceedings of the IEEE/CVF conference on computer vision and pattern recognition*, pages 2437–2445, 2020. 7
- [30] Takeru Miyato, Toshiki Kataoka, Masanori Koyama, and Yuichi Yoshida. Spectral normalization for generative adversarial networks. In *ICLR*, 2018. 5, 11

- [31] Didrik Nielsen, Priyank Jaini, Emiel Hoogeboom, Ole Winther, and Max Welling. Survae flows: Surjections to bridge the gap between vaes and flows. In *NeurIPS*, 2020. 5, 7
- [32] Erik Nijkamp, Ruiqi Gao, Pavel Sountsov, Srinivas Vasudevan, Bo Pang, Song-Chun Zhu, and Ying Nian Wu. MCMC should mix: Learning energy-based model with neural transport latent space MCMC. In *International Conference on Learning Representations*, 2022. 5
- [33] Kancharla Parimala and Sumohana Channappayya. Quality aware generative adversarial networks. In *Advances in Neural Information Processing Systems*, pages 2948–2958, 2019. 6
- [34] Gaurav Parmar, Dacheng Li, Kwonjoon Lee, and Zhuowen Tu. Dual contradistinctive generative autoencoder. In *Proceedings of the IEEE/CVF Conference on Computer Vision and Pattern Recognition (CVPR)*, pages 823–832, 2021. 1, 5, 6, 11
- [35] Stanislav Pidhorskyi, Donald A Adjeroh, and Gianfranco Doretto. Adversarial latent autoencoders. In *Proceedings of the IEEE/CVF Conference on Computer Vision and Pattern Recognition*, pages 14104–14113, 2020. 6
- [36] Yang Song and Stefano Ermon. Generative modeling by estimating gradients of the data distribution. In *Advances in Neural Information Processing Systems*, pages 11918–11930, 2019. 5
- [37] Yang Song and Stefano Ermon. Improved techniques for training score-based generative models. *arXiv preprint arXiv:2006.09011*, 2020. 6
- [38] Yang Song, Prafulla Dhariwal, Mark Chen, and Ilya Sutskever. Consistency models. 2023. 2, 5
- [39] Jakub M. Tomczak and Max Welling. VAE with a vampprior. In *International Conference on Artificial Intelligence and Statistics, AISTATS 2018, 9-11 April 2018, Playa Blanca, Lanzarote, Canary Islands, Spain*, pages 1214–1223. PMLR, 2018. 1
- [40] Eric Tzeng, Judy Hoffman, Kate Saenko, and Trevor Darrell. Adversarial discriminative domain adaptation. In *Proceedings of the IEEE conference on computer vision and pattern recognition*, pages 7167–7176, 2017. 1
- [41] Arash Vahdat and Jan Kautz. NVAE: A deep hierarchical variational autoencoder. In *Neural Information Processing Systems (NeurIPS)*, 2020. 1, 2, 5, 6, 7
- [42] Yinhuai Wang, Jiwen Yu, and Jian Zhang. Zero-shot image restoration using denoising diffusion null-space model. In *International Conference on Learning Representations*, 2023. 5, 7
- [43] Zhisheng Xiao, Karsten Kreis, Jan Kautz, and Arash Vahdat. Vaebm: A symbiosis between variational autoencoders and energy-based models. In *International Conference on Learning Representations*, 2021. 2, 5, 6, 7, 8
- [44] Jianwen Xie, Yang Lu, Song-Chun Zhu, and Yingnian Wu. A theory of generative convnet. In *International Conference on Machine Learning*, pages 2635–2644, 2016. 1
- [45] Jianwen Xie, Yang Lu, Ruiqi Gao, and Ying Nian Wu. Cooperative learning of energy-based model and latent variable model via mcmc teaching. In *Proceedings of the AAAI Conference on Artificial Intelligence*, 2018. 2
- [46] Jianwen Xie, Zilong Zheng, and Ping Li. Learning energy-based model with variational auto-encoder as amortized sampler. In *Proceedings of the AAAI Conference on Artificial Intelligence*, pages 10441–10451, 2021.
- [47] Jianwen Xie, Yaxuan Zhu, Jun Li, and Ping Li. A tale of two flows: Cooperative learning of langevin flow and normalizing flow toward energy-based model. In *International Conference on Learning Representations*, 2022. 2, 5, 7
- [48] Guandao Yang, Xun Huang, Zekun Hao, Ming-Yu Liu, Serge Belongie, and Bharath Hariharan. Pointflow: 3d point cloud generation with continuous normalizing flows. In *Proceedings of the IEEE/CVF international conference on computer vision*, pages 4541–4550, 2019. 1
- [49] Fisher Yu, Ari Seff, Yinda Zhang, Shuran Song, Thomas Funkhouser, and Jianxiong Xiao. Lsun: Construction of a large-scale image dataset using deep learning with humans in the loop. *arXiv preprint arXiv:1506.03365*, 2015. 5

A. Pseudo Code of Training Algorithm

Algorithm 1: Energy Calibrated Generative Model Algorithm.

input : Learning iterations T , number of MCMC steps K , observed examples $\{\mathbf{x}_i\}_{i=1}^n$, network optimizer \mathcal{Q} .

output: Estimated parameters ϕ, ω .

for $t = 0 : T - 1$ **do**

Primal-Step:

1. **Mini-batch:** Sample observed examples $\{\mathbf{x}_i\}_{i=1}^m$
2. **Mini-batch:** Sample generated examples $\{\hat{\mathbf{x}}_i\}_{i=1}^m$
3. **Sample $\tilde{\mathbf{x}}$ by MCMC:** For each generated $\hat{\mathbf{x}}_i$, sample $\tilde{\mathbf{x}}_i$ using Eq. (6) for K steps
4. **Learning E_ω :** $\omega_{t+1} = \mathcal{Q}(\nabla_{\omega_t} \hat{\mathcal{L}}(\omega_t), \omega_t)$
5. **Learning and Calibrating Generative Model ϕ_t :**
 $\phi_{t+1} = \mathcal{Q}(\nabla_{\phi_t} \hat{\mathcal{L}}(\phi_t) + \lambda \nabla_{\phi_t} \hat{\mathcal{L}}_{\text{con}}(\phi_t), \phi_t)$

Dual-Step:

6. **Update λ :** update λ according to Eq. (13)

B. More Details in zero-shot image restoration

Typical image restoration tasks usually have simple \mathbf{A} and \mathbf{A}^\dagger , we give some examples following:

Colorization: $\mathbf{A} = [1/3, 1/3, 1/3]$ converts each RGB channel pixel $[r, g, b]^T$ into a grayscale value $[r/3 + g/3 + b/3]$. A simple pseudo-inverse \mathbf{A}^\dagger is $\mathbf{A}^\dagger = [1, 1, 1]^T$, that satisfies $\mathbf{A}\mathbf{A}^\dagger\mathbf{A} = \mathbf{A}$.

Super Resolution: For SR with scale n , we can set $\mathbf{A} \in \mathbb{R}^{1 \times n^2}$ as a average-pooling operator $[1/n^2, \dots, 1/n^2]$. A simple pseudo-inverse $\mathbf{A}^\dagger \in \mathbb{R}^{n^2 \times 1}$ is $\mathbf{A}^\dagger = [1, \dots, 1]^T$.

Inpainting: For \mathbf{A} is a mask operator, simply let $\mathbf{A}^\dagger = \mathbf{A}$, we can have $\mathbf{A}\mathbf{A}^\dagger\mathbf{A} = \mathbf{A}$.

C. Additional Results in image generation

We present the performance of **Calibrated VAE** on STL-10 here. As shown in Tab. 8, we outperform DC-VAE and other adversarial baselines.

D. Experiment setting details in image generation

Evaluation Metric: We employ the FID score as the metric in most experiments. We compute the FID score between 50k generated samples and training images. On CelebA HQ we compute 30k generated samples and training images due to the dataset only containing 30k images.

Hyper-parameters: Given a large number of datasets, heavy compute requirements, and limited computational resources, we don't optimize the hyper-parameters carefully. Even if the backbone is not carefully selected or designed,

Model	FID↓
DC-VAE [34]	41.91
ProbGAN [11]	46.7
SN-GAN [30]	40.1
AutoGAN [8]	31.0
Calibrated VAE	14.24

Table 8. Generative performance on STL-10.

it's expected that we can use other well-designed backbones to easily get better results. Also, we just roughly choose the learning rate from 1e-4 or 2e-4 in all experiments. We use a Tanh to constrain the range of estimated μ by encoder f_α . For all other training details (e.g., detailed model architecture), we refer readers to our full code, which will be released after published.

E. Experiment details in Zero-Shot Image Restoration

We use the well-trained **Calibrated VAE** in zero-shot image restoration by the proposed application method in Sec. 3.6 with 100 MCMC steps.

F. Experiment setting details in ablation study

The same architectural design is consistently applied across all variants in our ablation studies. We employed a replay buffer of 10,000 for training the EBM, with a distribution of 5% sampling from noise and 95% sampling from the replay buffer. Regarding the EBM initiated with VAE samples, a similar approach was adopted, utilizing the same replay buffer size of 10,000, 5% sampling from the VAE, and 95% sampling from the replay buffer. Notably, in the absence of a replay buffer during the training of the EBM initiated with VAE samples, we were unable to produce reasonable generation outcomes.

G. Qualitative Comparison to Other models

We provide a qualitative comparison to other models on CIFAR-10 in Fig. 5. We use the official checkpoint from CoopFlow to generate its samples and use its official code to compute the corresponding FID score. For VAE BM w/o MCMC, we take the samples from its paper's appendix.

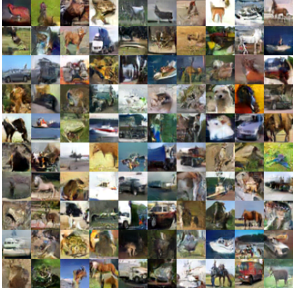
Please see if drop MCMC steps at test time sampling, how better our proposed method is compared to previous cooperative learning model (i.e., CoopFlow) and previous work that combines generative model and EBMs (i.e., VAE BM). And we note that CoopFlow is the most advanced model among existing cooperative learning models. Also, many existing works (e.g., CoopFlow and VAE BM) related to EBMs need extra hyper-parameters tuning stage to achieve high performance or will lead to a significantly



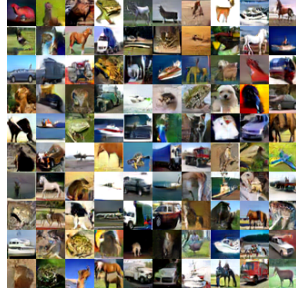
(a) CoopFlow without MCMC (FID=79.45)



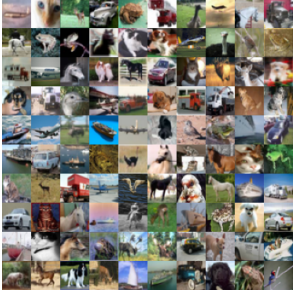
(b) VAE without MCMC (i.e., NVAE, FID=50.97)



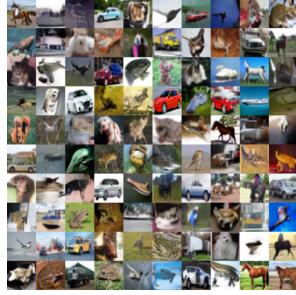
(c) CoopFlow w/o extra tuning hyper-parameters (FID=26.54)



(d) CoopFlow w/ carefully tuned hyper-parameters (FID=15.80)



(e) Real Data



(f) **Calibrated VAE** (FID=8.02)

Figure 5. Qualitative comparison of Energy Calibrated Generative Model (Ours) and other models on CIFAR-10. Samples are unselected.

worse result. And it can be seen in Fig. 5d that after carefully tuning the hyper-parameters, although the FID is better than the untuned, the color of samples by CoopFlow tends to be over-saturated, which is not the property of real data. In contrast, our proposed Energy Calibrated Generative Model can even drop MCMC steps at test time sampling while achieving high-quality samples.